

StreamDiffusion: A Pipeline-level Solution for Real-time Interactive Generation

Akio Kodaira^{1,*} Chenfeng Xu^{1,*} Toshiki Hazama^{1,*} Takanori Yoshimoto² Kohei Ohno³
 Shogo Mitsuhashi⁴ Soichi Sugano⁵ Hanying Cho⁶ Zhijian Liu⁷ Kurt Keutzer¹

¹UC Berkeley ²University of Tsukuba ³International Christian University
⁴Toyo University ⁵Tokyo Institute of Technology ⁶Tohoku University ⁷MIT

{akio.kodaira, xuchenfeng}@berkeley.edu

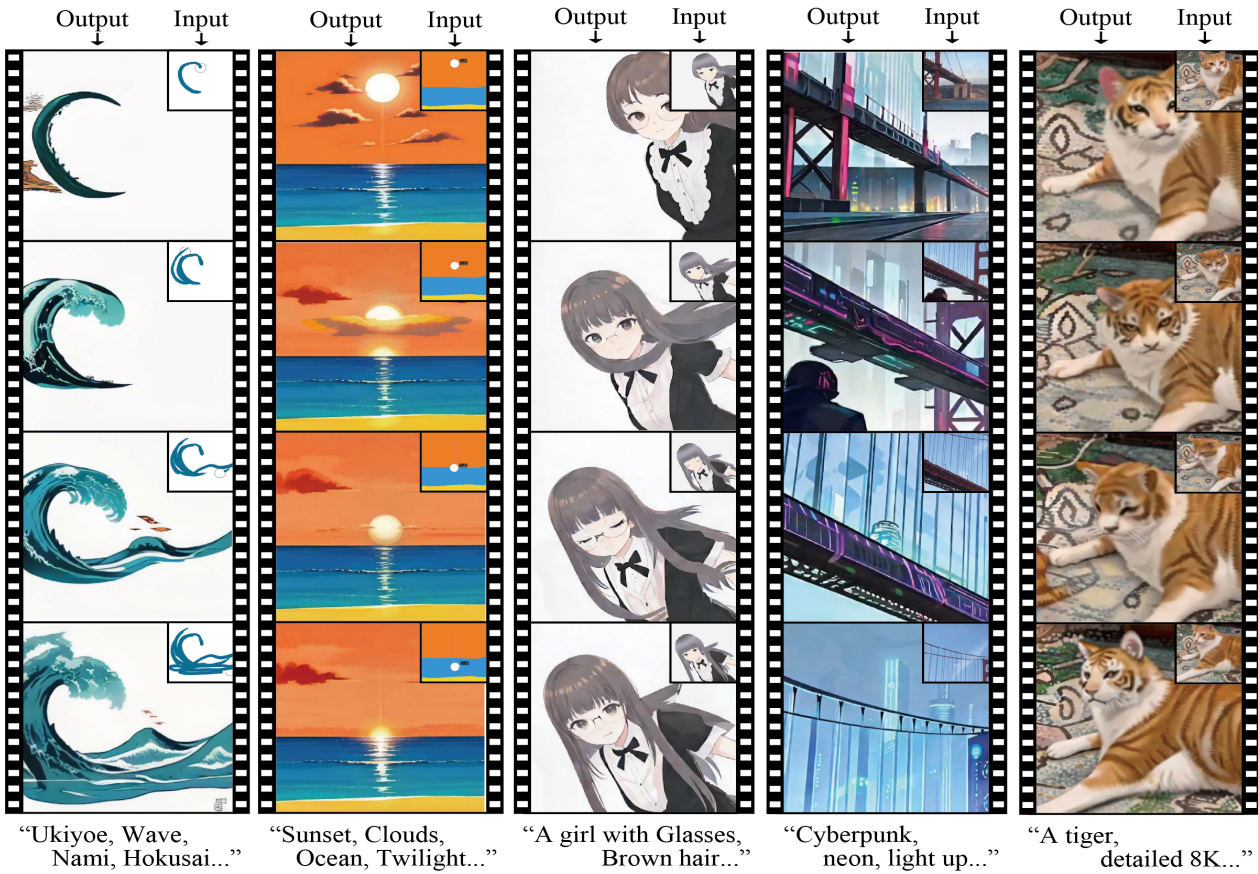


Figure 1. Real-time image-to-image results from camera and screen captures. The first and second columns show examples of AI-assisted drawing in real-time, and the third column displays the real-time rendering of 2D illustrations from 3D avatars. The fourth and fifth columns demonstrate the real-time camera filter.

Abstract

We introduce StreamDiffusion, a real-time diffusion pipeline designed for interactive image generation. Exist-

ing diffusion models are adept at creating images from text or image prompts, yet they often fall short in real-time interaction. This limitation becomes particularly evident in scenarios involving continuous input, such as Metaverse, video game graphics rendering, live video streaming, and broadcasting, where high throughput is imperative. To ad-

* denotes equal contribution

This work was done when Toshiki was a remote intern at UC Berkeley

dress this, we present a novel and simple approach that transforms the original sequential denoising into the batching denoising process. Stream Batch eliminates the conventional wait-and-interact approach and enables fluid and high throughput streams. To handle the disparity in frequencies between data input and model throughput, we design a novel input-output queue for parallelizing the streaming process. Moreover, the existing diffusion pipeline uses classifier-free guidance to enforce the generated results conditioned on the prompts. We point out that current implementations are inefficient due to the inherent redundancy of negative conditional denoising. To mitigate the redundant computations, we propose a novel residual classifier-free guidance (RCFG) algorithm that reduces the number of negative conditional denoising steps to only one or even zero. Besides, to optimize power consumption, we use a simple and effective stochastic similarity filtering strategy, which significantly reduces GPU activation frequency, thereby improving GPU utilization efficiency. Our batching denoising strategy achieves around 1.5x speedup compared to the sequential denoising method at different denoising levels. The proposed (RCFG) leads to up-to 2.05x speedups compared to the previous conventional classifier-free guidance. The combination of the proposed strategies and existing mature acceleration tools makes the image-to-image generation achieve up-to 91.07fps on one RTX 4090 GPU, improving the throughputs of AutoPipeline developed by Diffusers over 59.56x. Beyond the pipeline efficiency, our proposed StreamDiffusion also significantly reduces the energy consumption by 2.39x on one RTX 3060 GPU and 1.99x on one RTX 4090 GPU for a static scene input, respectively. The code is available at <https://github.com/cumulo-autumn/StreamDiffusion>.

1. Introduction

Recently, there has been a growing trend in the commercialization of diffusion models [3, 21, 23] for applications within the Metaverse, as well as in the realms of online video streaming and broadcasting. These areas require diffusion pipelines that offer high throughput and low latency to ensure efficient human interaction. A pertinent example is the use of diffusion models to create virtual YouTubers. These digital personas should be capable of reacting in a fluid and responsive manner to user input.

To advance high throughput and real-time interactive capabilities, current efforts primarily focus on reducing the number of denoising iterations, such as decreasing from 50 iterations to just a few [16, 17] or even one [13, 28]. The common strategy is to distill the multi-step diffusion models into a few steps or re-frame the diffusion process with neural Ordinary Differential Equations (ODE) [14, 26]. Quantization has also been applied to diffusion models [9, 12] to

improve efficiency.

In this paper, we start from an orthogonal direction and introduce StreamDiffusion, a pipeline-level solution that enables real-time interactive image generation with high throughput. We highlight that existing model design efforts can still integrate with our pipeline. Our approach enables the use of N-step denoising diffusion models while still keeping high throughput and offers users more flexibility in choosing their preferred models.

We leverage a simple strategy in StreamDiffusion: instead of the original sequential denoising mode, we batch the denoising steps. We are inspired by the asynchronous processing in the computer architecture pipeline, and point out that we do not need to wait for the previous denoising processes to finish then to start the current denoising step, as shown in Fig. 2. In order to deal with the synchronous issue of input frequency and U-Net processing frequency, we leverage a queue strategy to cache the inputs and output. Our pipeline is different from merely asynchronous processing. We make use of the advantage of GPU parallelism; thus, we can use one U-Net to denoise a batched noise latent feature. More importantly, the existing diffusion pipeline incorporated classifier-free guidance to emphasize the given prompts in the generated images. Nevertheless, traditional implementations of classifier-free guidance are plagued by excessive and redundant computational overheads. We introduce an innovative approach termed as *residual classifier-free guidance (RCFG)*. The novel technique approximates the negative condition with a virtual residual noise, which allows us to calculate the negative condition noise only during the initial step of the process.

Further, we point out that maintaining the diffusion models always in an interactive mode is energy-consuming as it keeps hitting GPU. To reduce the energy, we further apply a stochastic similarity filtering strategy. In the pipeline, we compute the similarities between continuous inputs and determine whether the diffusion model should process the images based on the similarity.

Experiments demonstrate that our proposed StreamDiffusion can achieve up to 91.07fps for image generation on a one RTX4090 GPU, surpassing the diffusion Autopipeline from Diffusers team by up to 59.6x. Besides, our stochastic similarity filtering strategy significantly reduces the GPU power usage by 2.39x on one RTX 3090GPU and by 1.99x on one RTX 4090GPU. Our proposed StreamDiffusion is a new diffusion pipeline that is not only efficient but also energy-saving.

2. Related works

2.1. Diffusion Models

Diffusion models, as introduced in [8, 25], have sparked considerable interest in the commercial sector due to their

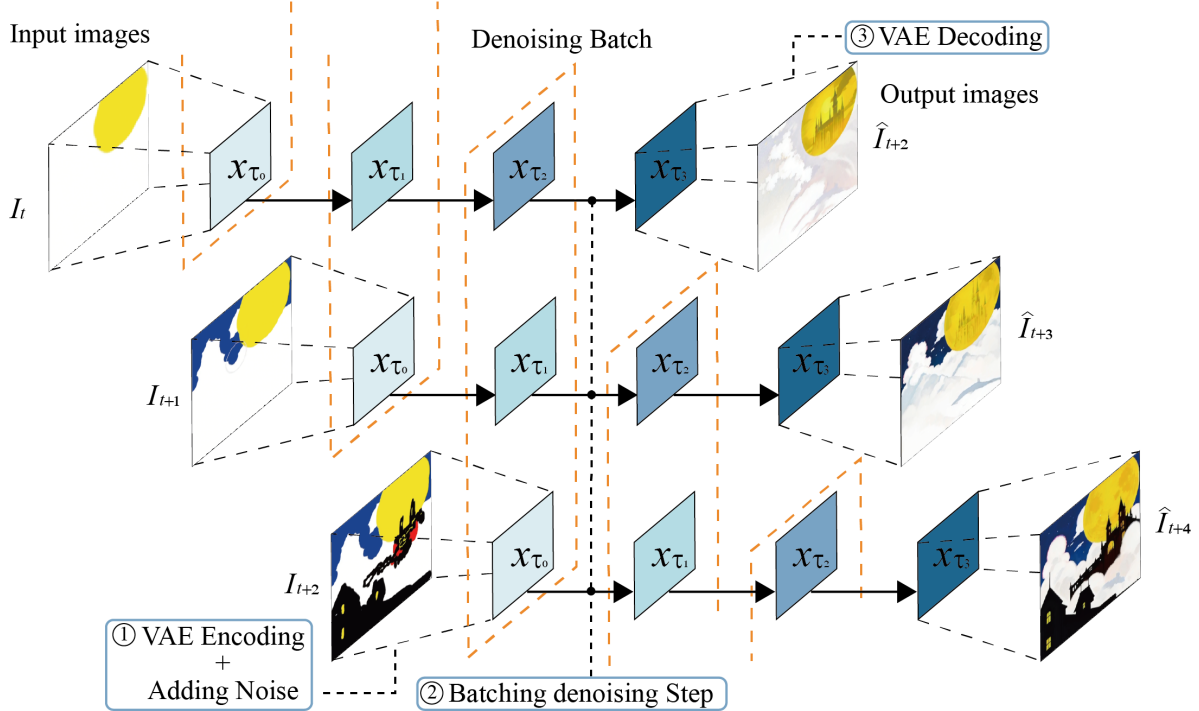


Figure 2. The concept of Stream Batch. In our approach, instead of waiting for a single image to be fully denoised before processing the next input image, we accept the next input image after each denoising step. This creates a denoising batch where the denoising steps are staggered for each image. By concatenating these staggered denoising steps into a batch, we can efficiently process continuous inputs using a U-Net for batch processing. The input image encoded at timestep t is generated and decoded at timestep $t + n$, where n is the number of the denoising steps.

high-quality image generation capabilities and the level of control they offer over the generated images. These models have been progressively adapted for various applications, including text-to-image generation [2, 19, 20], image edition [1, 22], and video generation [4, 5].

A notable advancement in this area is the development of consistent models [26], which have demonstrated the potential to improve the efficiency of the sampling process with rarely compromising on image quality. Building on this, recent studies have focused on enhancing the efficiency of diffusion models by reducing the number of sampling steps required, further expanding their practical applicability and efficiency.

2.2. Accelerating Diffusion Model

Diffusion models are currently limited by their slow speed in generating outputs. To address this drawback, several strategies have been developed. These include methods that don't require additional training, like using Ordinary Differential Equation (ODE) solvers, as explored by [14, 15, 17, 26]. Other techniques involve adaptive step size solvers as discussed by [10] and predictor-corrector methods noted by [25]. The training-based methods are also proposed, such as optimized discretization techniques [27],

neural operator design [29], and model distillation [24]. Our proposed method distinguishes itself significantly from the approaches mentioned previously. While earlier methods primarily focus on the low latency of their individual model designs, our approach takes a different route. We introduce a comprehensive pipeline-level solution specifically tailored for high throughputs, which enables efficient interactive diffusion. Our pipeline is designed to seamlessly integrate most of the low-latency diffusion models discussed above. By doing so, we achieve a notable increase in speed within the interactive generation process.

3. StreamDiffusion Pipeline

StreamDiffusion is a new diffusion pipeline aiming for high throughput. It comprises several key components: the Stream Batch strategy, Residual Classifier-Free Guidance (RCFG), an input-output queue, Stochastic Similarity Filter, a pre-computation procedure, and model acceleration tools with a tiny-autoencoder. We elaborate on the details below.

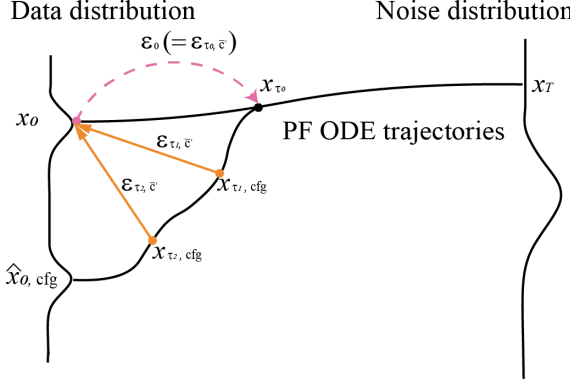


Figure 3. Virtual residual noise vectors: The orange vectors depict the virtual residual noise that starts from the PF ODE trajectory and points to the original input latent x_0

3.1. Batching the denoise step

In diffusion models, denoising steps are performed sequentially, resulting in a proportional increase in the processing time of U-Net relative to the number of steps. However, to generate high-fidelity images, it is necessary to increase the number of steps. To resolve the high-latency generation in interactive diffusion, we propose a method called Stream Batch.

The Stream Batch technique restructures sequential denoising operations into batched processes, wherein each batch corresponds to a predetermined number of denoising steps, as depicted in Fig. 2. The size of each batch is determined by the number of these denoising steps. This approach allows for each batch element to advance one step further in the denoising sequence via a single pass through U-Net. By iteratively applying this method, it is possible to effectively transform input images encoded at timestep t into their corresponding image-to-image results at timestep $t+n$, thereby streamlining the denoising procedure.

Stream Batch significantly reduces the need for multiple U-Net inferences. The processing time does not escalate linearly with the number of steps. This technique effectively shifts the trade-off from balancing processing time and generation quality to balancing VRAM capacity and generation quality. With adequate VRAM scaling, this method enables the production of high-quality images within the span of a single U-Net processing cycle, effectively overcoming the constraints imposed by increasing denoising steps.

3.2. Residual Classifier-Free Guidance

Classifier-free guidance (CFG) [7] is an algorithm that enhances the effect of the original conditioning by performing vector calculations between an unconditioning or a negative conditioning term [6] and the original conditioning term (Eq. 1).

$$\epsilon_{\tau_i, \text{cfg}} = \epsilon_{\tau_i, \bar{c}} + \gamma(\epsilon_{\tau_i, c} - \epsilon_{\tau_i, \bar{c}}), \quad (1)$$

where $\epsilon_{\tau_i, c}$ and $\epsilon_{\tau_i, \bar{c}}$ are predicted residual noise at the denoising step τ_i with conditioning embedding c and negative conditioning embedding \bar{c} , respectively, and γ is a guidance scale.

This allows for benefits such as strengthening the effect of the prompt. However, to compute the negative conditioning residual noise, it is necessary to pair each input latent variable with the negative conditioning embedding and pass it through the U-Net at every inference time. To address this drawback, we introduce Residual Classifier-Free Guidance (RCFG), which significantly reduces the computational cost of the additional U-Net inference for the negative conditioning embedding.

Firstly, the encoded input latent x_0 can be transferred to the noise distribution x_{τ_0} as follows,

$$x_{\tau_0} = \sqrt{\alpha_{\tau_0}} x_0 + \sqrt{\beta_{\tau_0}} \epsilon_0, \quad (2)$$

where α_{τ_0} and β_{τ_0} are values determined by a noise scheduler and ϵ_0 is a sampled noise from a Gaussian $\mathcal{N}(0, I)$. Following the implementation of latent consistency model [26], we can predict the data distribution $\hat{x}_{0, \tau_{i-1}, \text{cfg}}$ and generate a next step noise distribution $x_{\tau_i, \text{cfg}}$ using the CFG residual noise $\epsilon_{\tau_{i-1}, \text{cfg}}$ as follows,

$$\hat{x}_{0, \tau_{i-1}, \text{cfg}} = \frac{x_{\tau_{i-1}, \text{cfg}} - \sqrt{\beta_{\tau_{i-1}}} \epsilon_{\tau_{i-1}, \text{cfg}}}{\sqrt{\alpha_{\tau_{i-1}}}} \quad (3)$$

$$x_{\tau_i, \text{cfg}} = \sqrt{\alpha_{\tau_i}} \hat{x}_{0, \tau_{i-1}, \text{cfg}} + \sqrt{\beta_{\tau_i}} \epsilon_i, \quad (4)$$

Where $\epsilon_i \sim \mathcal{N}(0, I)$.

For the next step CFG calculation, instead of computing the next step negative conditioning residual noise $\epsilon_{\tau_i, \bar{c}}$, which requires an additional U-Net computation cost, we hypothesize the existence of virtual residual noise $\epsilon_{\tau_i, \bar{c}'}$, and a virtual negative condition embedding \bar{c}' that predicts the original input image's latent x_0 from $x_{\tau_i, \text{cfg}}$, as shown in Fig. 3. Similarly to Eq. 3, this virtual residual noise satisfies Eq. 5 to predict the input latent x_0 .

$$x_0 \approx \hat{x}_{0, \tau_i, \bar{c}'} = \frac{x_{\tau_i, \text{cfg}} - \sqrt{\beta_{\tau_i}} \epsilon_{\tau_i, \bar{c}'}}{\sqrt{\alpha_{\tau_i}}} \quad (5)$$

Given the initial value x_0 , and the subsequent values of $x_{\tau_i, \text{cfg}}$ obtained sequentially through Eq. 4, the virtual residual noise $\epsilon_{\tau_i, \bar{c}'}$ can be analytically determined by employing these values with the Eq. 5:

$$\epsilon_{\tau_i, \bar{c}'} = \frac{x_{\tau_i, \text{cfg}} - \sqrt{\alpha_{\tau_i}} x_0}{\sqrt{\beta_{\tau_i}}} \quad (6)$$

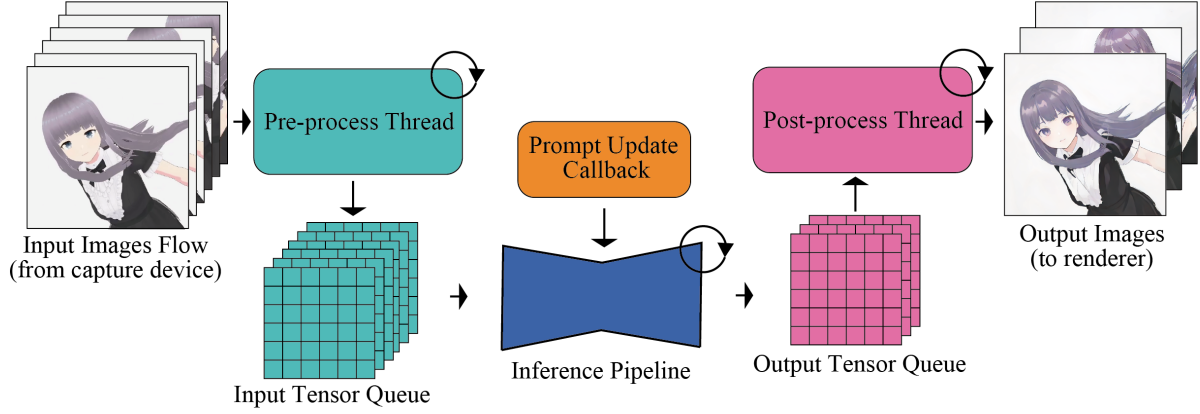


Figure 4. Input-Output Queue: The process of converting input images into a tensor data format manageable by the pipeline, and conversely, converting decoded tensors back into output images requires a non-negligible amount of additional processing time. To avoid adding these image processing times to the bottleneck process, the neural network inference process, we have segregated image pre-processing and post-processing into separate threads, allowing for parallel processing. Moreover, by utilizing an Input Tensor Queue, we can accommodate temporary lapses in input images due to device malfunctions or communication errors, enabling smooth streaming.

With the virtual residual noise $\epsilon_{\tau_i, \bar{c}'}$ obtained from Eq. 6, we formulate RCFG as follows,

$$\epsilon_{\tau_i, \text{cfg}} = \delta \epsilon_{\tau_i, \bar{c}'} + \gamma (\epsilon_{\tau_i, c} - \delta \epsilon_{\tau_i, \bar{c}'}) \quad (7)$$

where δ is a magnitude moderation coefficient for the virtual residual noise that softens the effect and the approximation error of the virtual residual noise.

RCFG that uses the original input image latent x_0 as the residual term can effectively generate results that diverge from the original input image according to the magnitude of the guidance scale γ , thereby enhancing the effect of conditioning without the need for additional U-Net computations. We call this method Self-Negative RCFG.

Not only to deviate from the original input image x_0 , but also to diverge from any negative condition, we can compute the negative conditioning residual noise $\epsilon_{\tau_0, \bar{c}}$ using U-Net only onetime for the first denoising step and use this to predict the negative conditioning denoised data as follows,

$$\hat{x}_{0, \tau_0, \bar{c}} = \frac{x_{\tau_0} - \sqrt{\beta_{\tau_0}} \epsilon_{\tau_0, \bar{c}}}{\sqrt{\alpha_{\tau_0}}} \quad (8)$$

In Eq. 6, instead of x_0 , using $\hat{x}_{0, \tau_0, \bar{c}}$, we can obtain the virtual residual noise $\epsilon_{\tau_{i+1}, \bar{c}'}$ that can effectively diverge the generation results from the controllable negative conditioning embedding \bar{c} . We call this Onetime-Negative RCFG.

By combining Eq. 2, Eq. 6, and Eq. 8, both Self-Negative RCFG and Onetime-Negative RCFG can be uniformly represented by the following equation,

$$\epsilon_{\tau_i, \bar{c}'} = \frac{x_{\tau_i, \text{cfg}} - \sqrt{\alpha_{\tau_i}} x_0}{\sqrt{\beta_{\tau_i}}} + \sqrt{\frac{\alpha_{\tau_i} \beta_{\tau_0}}{\beta_{\tau_i} \alpha_{\tau_0}}} (\epsilon_{\tau_0, \bar{c}} - \epsilon_0) \quad (9)$$

When $\epsilon_{\tau_0, \bar{c}} = \epsilon_0$, Eq. 9 is identical to Eq. 6 and returns Self-Negative RCFG result.

In contrast to the conventional CFG, which requires $2n$ computations of U-Net, the Self-Negative RCFG and Onetime-Negative RCFG necessitate only n and $n+1$ computations of U-Net, respectively, where n is the number of the denoising steps.

3.3. Input-Output Queue

The current bottleneck in high-speed image generation systems lies in the neural network modules, including VAE and U-Net. To maximize the overall system speed, processes such as pre-processing and post-processing of images, which do not require handling by the neural network modules, are moved outside of the pipeline and processed in parallel.

In the context of input image handling, specific operations, including resizing of input images, conversion to tensor format, and normalization, are meticulously executed. To address the disparity in processing frequencies between the human inputs and the model throughput, we design an input-output queuing system to enable efficient parallelization, as shown in Fig. 4. This system operates as follows: processed input tensors are methodically queued for Diffusion Models. During each frame, Diffusion Model retrieves the most recent tensor from the input queue and forwards it to the VAE Encoder, thereby triggering the image generation sequence. Correspondingly, tensor outputs from the VAE Decoder are fed into an output queue. In the subsequent output image handling phase, these tensors are subject to a series of post-processing steps and conversion into the appropriate output format. Finally, the fully processed image data is transmitted from the output handling system

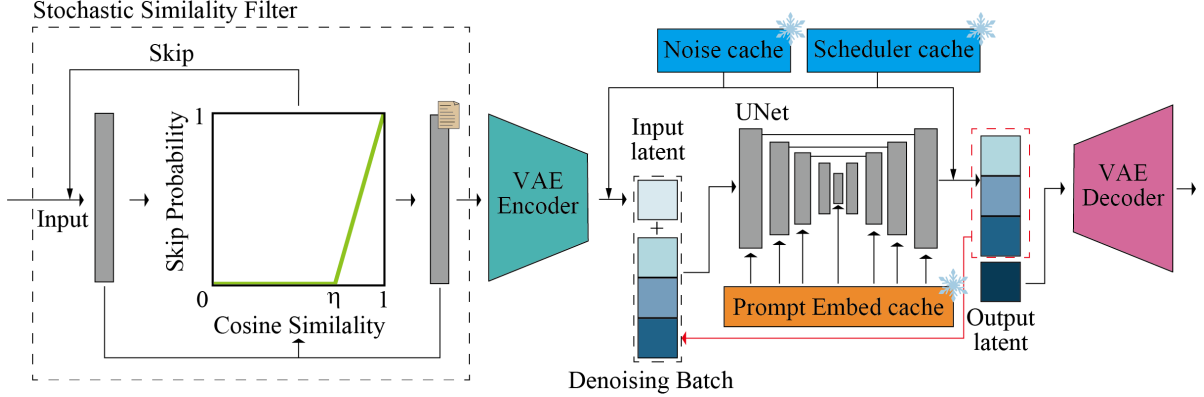


Figure 5. Inference pipeline overview: The core diffusion inference pipeline, including VAE and U-Net. By incorporating a denoising batch and pre-computed prompt embedding cache, sampled noise cache, and scheduler values cache, the inference pipeline is enhanced in terms of speed and enables real-time image generation. Stochastic Similarity Filter (SSF) is designed to save GPU power usage. It dynamically gates the pass of the diffusion model. This framework realizes fast and energy-efficient real-time inference.

to the rendering client.

3.4. Stochastic Similarity Filter

When images remain unchanged or show minimal changes, particularly in scenarios without active user interaction or static environment, nearly identical input images are often repeatedly fed into the VAE and U-Net. This leads to the generation of identical or nearly identical images and unnecessary consumption of GPU resources. In contexts involving continuous inputs, such instances of unmodified input images can occasionally occur. To tackle this issue and minimize unnecessary computational load, we propose a strategy termed *stochastic similarity filter (SSF)*, as shown in Fig. 5.

We calculate the cosine similarity between the current input Image I_t and the past reference frame Image I_{ref} .

$$S_C(I_t, I_{\text{ref}}) = \frac{I_t \cdot I_{\text{ref}}}{\|I_t\| \|I_{\text{ref}}\|} \quad (10)$$

Based on this cosine similarity, we calculate the probability of skipping the subsequent VAE and U-Net processes. It is given by

$$P(\text{skip}|I_t, I_{\text{ref}}) = \max \left\{ 0, \frac{S_C(I_t, I_{\text{ref}}) - \eta}{1 - \eta} \right\}, \quad (11)$$

where η is the similarity threshold. This probability decides whether subsequent processes like VAE Encoding, U-Net, and VAE Decoding should be skipped or not. If not skipped, the input image at that time is saved and updated as the reference image I_{ref} for future use. This probabilistic skipping mechanism allows the network to operate fully in dynamic scenes with low inter-frame similarity, while in static scenes with high inter-frame similarity, the network's operational rate decreases, conserving computational resources.

The GPU usage is modulated seamlessly based on the similarity of the input images, enabling smooth adaptation to scenes with varying dynamics.

Note: We emphasize that compared to determine whether we skip the compute via a hard threshold, the proposed probability-sampling-based similarity filtering strategy leads to a more smooth video generation. Because the hard threshold is prone to making the video stuck which hurts the impression of watching video streaming, while the sampling-based method significantly improves the smoothness.

3.5. Pre-computation

The U-Net architecture requires both input latent variables and conditioning embeddings. Typically, the conditioning embedding is derived from a prompt embedding, which remains constant across different frames. To optimize this, we pre-compute the prompt embedding and store it in a cache. In interactive or streaming mode, this pre-computed prompt embedding cache is recalled. Within U-Net, the Key and Value are computed based on this pre-computed prompt embedding for each frame. We have modified the U-Net to store these Key and Value pairs, allowing them to be reused. Whenever the input prompt is updated, we recompute and update these Key and Value pairs inside U-Net.

For consistent input frames across different timesteps and to improve computational efficiency, we pre-sample Gaussian noise for each denoising step and store it in the cache. This ensures that while each denoising step has distinct noise, every timestep retains the same noise ($x_{t,\tau} \neq x_{t,\tau+1}$ and $x_{t+1,\tau} = x_{t,\tau}$). This approach is particularly relevant for image-to-image tasks.

We also precompute α_τ and β_τ , the noise strength coefficients for each denoising step τ , defined as:

$$x_t = \sqrt{\alpha_\tau} x_0 + \sqrt{\beta_\tau} \epsilon \quad (12)$$

This is a minor point in low throughput scenarios, but at frame rates higher than 60 FPS, the overhead of recomputing these static values becomes noticeable. If we achieve 60 FPS (i.e. 16.666 ms) with recomputing these static values in the loop with pre-computed cache, we can achieve 62 FPS (i.e. 16.066 ms).

We note that we have a specific design of key-value cache for Latent Consistency Models (LCM). As per the original paper, we need to compute $c_{\text{skip}}(\tau)$ and $c_{\text{out}}(\tau)$ to satisfy the following equation:

$$f_\theta(x, \tau) = c_{\text{skip}}(\tau)x + c_{\text{out}}(\tau)F_\theta(x, \tau). \quad (13)$$

The functions $c_{\text{skip}}(\tau)$ and $c_{\text{out}}(\tau)$ in original LCM [17] is constructed as follows:

$$c_{\text{skip}}(\tau) = \frac{\sigma_{\text{data}}^2}{(s\tau)^2 + \sigma_{\text{data}}^2}, \quad c_{\text{out}}(\tau) = \frac{\sigma_{\text{data}} s \tau}{\sqrt{\sigma_{\text{data}}^2 + (s\tau)^2}}, \quad (14)$$

where $\sigma_{\text{data}} = 0.5$, and the timestep scaling factor $s = 10$. We note that with $s = 10$, $c_{\text{skip}}(\tau)$ and $c_{\text{out}}(\tau)$ approximate delta functions that enforce the boundary condition to the consistency models. (i.e., at denoising step $\tau = 0$, $c_{\text{skip}}(0) = 1$, $c_{\text{out}}(0) = 0$; and at $\tau \neq 0$, $c_{\text{skip}}(\tau) = 0$, $c_{\text{out}}(\tau) = 1$). At inference time, there's no need to recompute these functions repeatedly. We can either pre-compute $c_{\text{skip}}(\tau)$ and $c_{\text{out}}(\tau)$ for all denoising steps τ in advance or simply use constant values $c_{\text{skip}} = 0$, $c_{\text{out}} = 1$ for any arbitrary denoising step τ .

3.6. Model Acceleration and Tiny AutoEncoder

We employ TensorRT to construct the U-Net and VAE engines, further accelerating the inference speed. TensorRT is an optimization toolkit from NVIDIA that facilitates high-performance deep learning inference. It achieves this by performing several optimizations on neural networks, including layer fusion, precision calibration, kernel auto-tuning, dynamic tensor memory, and more. These optimizations are designed to increase throughput and efficiency for deep learning applications.

To optimize speed, we configured the system to use static batch sizes and fixed input dimensions (height and width). This approach ensures that the computational graph and memory allocation are optimized for a specific input size, leading to faster processing times. However, this means that if there is a requirement to process images with different shapes (i.e., varying heights and widths) or to use different batch sizes (including those for denoising steps),

a new engine tailored to these specific dimensions must be built. This is because the optimizations and configurations applied in TensorRT are specific to the initially defined dimensions and batch size, and changing these parameters would necessitate a reconfiguration and re-optimization of the network within TensorRT.

Besides, we employ a tiny AutoEncoder, which has been engineered as a streamlined and efficient counterpart to the traditional Stable Diffusion AutoEncoder [11, 20]. TAESD excels in rapidly converting latents into full-size images and accomplishing decoding processes with significantly reduced computational demands.

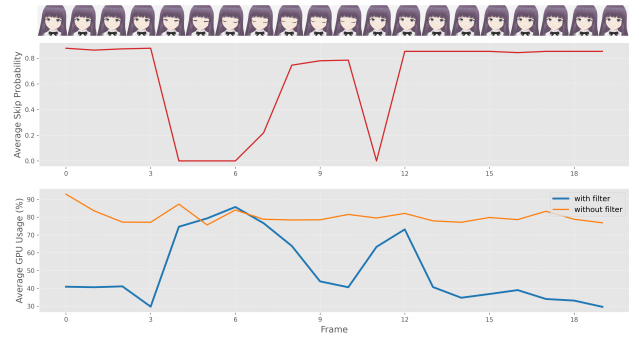


Figure 6. GPU Usage comparison under static scene. (GPU: RTX3060, Number of frames: 20) The blue line represents the GPU usage with SSF, the orange line indicates GPU usage without SSF, and the red line denotes the Skip probability calculated based on the cosine similarity between input frames. Additionally, the top of the plot displays input images corresponding to the same timestamps. In this case, the character in the input images is only blinking. Thus, this analysis compares GPU usage in a static scenario.

4. Experiments

We implement StreamDiffusion pipeline upon LCM, LCM-LoRA [17, 18] and SD-turbo [21]. As a model accelerator, we use TensorRT and for the light weight efficient VAE we use TAESD [11]. Our pipeline is compatible to the consumer GPU. We test our pipeline on NVIDIA RTX4090 GPU, Intel Core i9-13900K CPU, Ubuntu22.04.3 LTS, and NVIDIA RTX3060 GPU, Intel Core i7-12700K, Windows11 for image generation. We note that we evaluate the throughput mainly via the average inference time per image through processing 100 images.

4.1. Quantitative Evaluation of Denoising Batch

The efficiency comparison between the denoising batch and the original sequential U-Net loop is shown in Fig. 8. When implementing a denoising batch strategy, we observe a significant improvement in processing time. It achieves a reduction by half when compared to a conventional U-Net

Table 1. Comparison of Average Inference Time at Different Denoising Steps with Speedup Factors. (GPU: NVIDIA RTX4090, CPU: Core i9-13900K, OS: Ubuntu22.04.3 LTS)

Denoising Step	StreamDiffusion (ms)	StreamDiffusion w/o TRT (ms)	AutoPipeline Image2Image (ms)
1	10.65 (59.6x)	21.34 (29.7x)	634.40 (1x)
2	16.74 (39.3x)	30.61 (21.3x)	652.66 (1x)
4	26.93 (25.8x)	48.15 (14.4x)	695.20 (1x)
10	62.00 (13.0x)	96.94 (8.3x)	803.23 (1x)

Table 2. Comparison of Average Inference Time at Different Denoising Steps among Different CFG Methods

Denoising Step	Self-Negative RCFG (ms)	Onetime-Negative RCFG (ms)	Normal CFG (ms)
1	11.04 (1.52x)	16.55 (1.01x)	16.74 (1x)
2	16.61 (1.64x)	20.64 (1.32x)	27.18 (1x)
3	20.64 (1.74x)	27.25 (1.32x)	35.91 (1x)
4	26.19 (1.90x)	31.65 (1.57x)	49.71 (1x)
5	31.47 (2.05x)	36.04 (1.79x)	64.64 (1x)

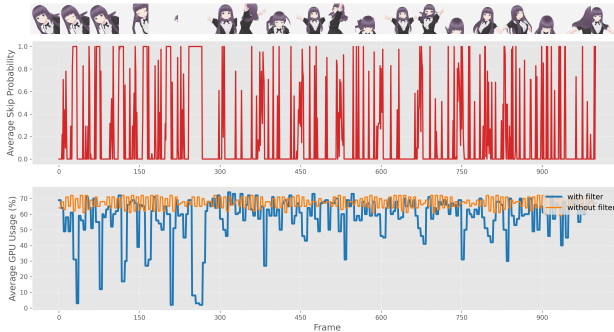


Figure 7. GPU Usage comparison under dynamic scene. (GPU: RTX4090, Number of frames: 1000) The blue line represents the GPU usage with SSF, the orange line indicates GPU usage without SSF, and the red line denotes the Skip probability calculated based on the cosine similarity between input frames. Additionally, the top of the plot displays input images corresponding to the same timestamps. In this case, the character in the input images keeps moving dynamically. Thus, this analysis compares GPU usage in a dynamic scenario.

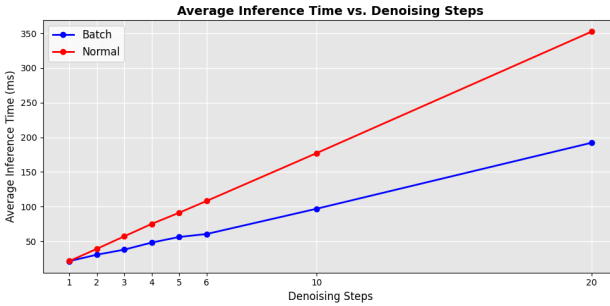


Figure 8. Average inference time comparison between Stream Batch and normal sequential denoising without TensorRT.

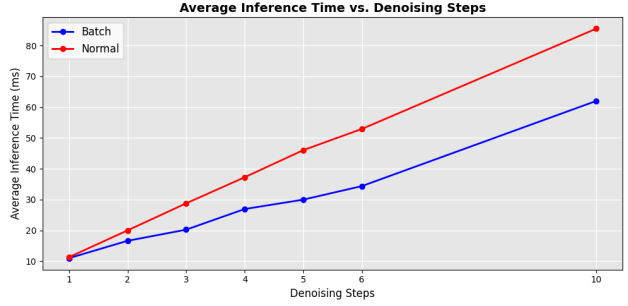


Figure 9. Average inference time comparison between Stream Batch and normal sequential denoising with using TensorRT

loop at sequential denoising steps. Even though applying TensorRT, the accelerate tool for neural modules, our proposed Stream Batch still boosts the efficiency of original sequential diffusion pipeline by a large margin at different denoising steps.

Besides, we compare our method with the AutoPipeline-ForImage2Image, which is a pipeline developed by Huggingface diffusers ¹. The average inference time comparison is presented in Table. 1. Our pipeline demonstrates a substantial speed increase. When we use TensorRT, StreamDiffusion achieves a minimum speed-up 13.0 times when running the 10 denoising steps, and reaching up to 59.6 times in scenarios when involving a single denoising step. Even though without TensorRT, StreamDiffusion achieves 29.7 times speed up compared to AutoPipeline when using one step denoising, and 8.3 times speedup at 10 step denoising.

Table. 2 presents a comparison of the inference times

¹<https://github.com/huggingface/diffusers>

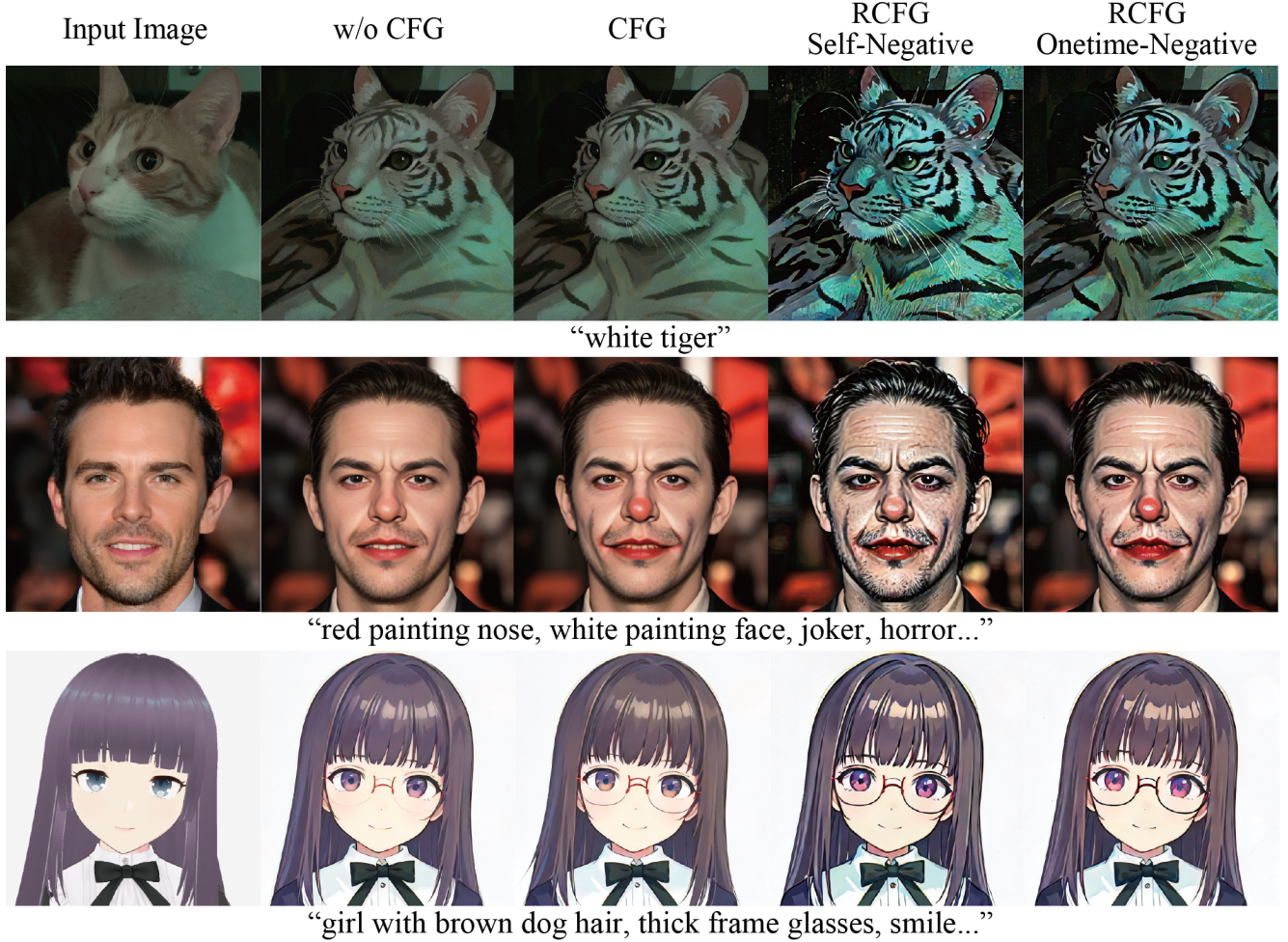


Figure 10. Results using no CFG, standard CFG, and RCFG with Self-Negative and Onetime-Negative approaches. When compared to cases where CFG is not utilized, the cases with CFG utilized can intensify the impact of prompts. In the proposed method RCFG, a more pronounced influence of prompts was observed. Both CFG and RCFG use guidance scale $\gamma = 1.4$. For RCFG, the first two rows use magnitude modulation coefficient $\delta = 1.0$, and the third row uses $\delta = 0.5$.

for StreamDiffusion pipelines with RCFG and conventional CFG. The additional computations required to apply Self-Negative RCFG are merely lightweight vector operations, resulting in negligible changes in inference time compared to when Self-Negative is not used. When employing Onetime-Negative RCFG, additional UNet computations are necessary for the first step of the denoising process. Therefore, One-time-negative RCFG and conventional CFG have almost identical inference times for a single denoising step case. However, as the number of denoising steps increases, the difference in inference time from conventional CFG to both Self-Negative and Onetime-Negative RCFG becomes more pronounced. At denoising step 5, a speed improvement of 2.05x is observed with Self-Negative RCFG and 1.79x with Onetime-Negative RCFG, compared to conventional CFG.

4.2. Energy Consumption

We then conduct a comprehensive evaluation of the energy consumption associated with our proposed stochastic similarity filter (SSF), as depicted in Figure. 6 and Figure. 7. These figures provide the GPU utilization patterns when SSF (Threshold η set at 0.98) is applied to input videos containing scenes with periodic static characteristics. The comparative analysis reveals that the incorporation of SSF significantly mitigates GPU usage in instances where the input images are predominantly static and demonstrate a high degree of similarity.

Figure. 6 delineates the results derived from a meticulously executed two-denoise-step img2img experiment. This experiment was conducted on a 20-frame video sequence, employing NVIDIA RTX3060 graphics processing units with or without the integration of SSF. The experiment

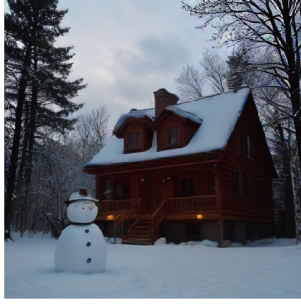
【Base model】+LCM-LoRA: 4 step denoising

【counterfeitV30】



“Girl with panda ears
wearing a hood...”

【Aziibereadlmix】



“Snowman, christmas,
tree, log house...”

【HimawariMix-v8】



“knight with a sword,
dark dragon...”

【PastelMix】



“a girl, hatsunemiku,
beautiful detail...”

【Van Gogh Likeness】



“A cat, animal,
beautiful eyes...”

【kohaku-v2.1】

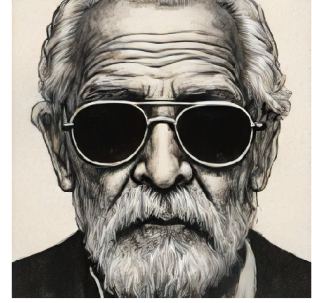


“A girl with pink hair,
stuffed toys, smiling...”

【sd-turbo】: 1 step denoising



“A cat with hat,
photorealistic, 8K...”



“old man, sunglasses,
ink painting style...”

Figure 11. Text-to-Image generation results. We use four step denoising for LCM-LoRA, and one step denoising for sd-turbo. Our StreamDiffusion enables the real-time generation of images with quality comparable to those produced using Diffusers AutoPipeline Text2Image.

results indicate a substantial decrease in average power consumption from **85.96w** to **35.91w** on one RTX3060 GPU. Using the same static scene input video with one NVIDIA RTX4090GPU, the power consumption was reduced from **238.68w** to **119.77w**.

Furthermore, Figure. 7 expounds on the findings from a similar two-denoise-step img2img experiment using one RTX4090GPU. This time the evaluation of energy consumption is performed on a 1000-frame video featuring dynamic scenes. Remarkably, even under drastically dynamic conditions, the SSF efficiently extracted several frames exhibiting similarity from the dynamic sequence. This process results in a noteworthy reduction in average power consumption, from **236.13w** to **199.38w**. These findings underscore the efficacy of the Stochastic Similarity Filter in enhancing energy efficiency, particularly in scenarios involving static or minimally varying visual content.

4.3. Ablation study

In our ablation study, as summarized in Table 3, we evaluate the average inference time of our proposed method under various configurations to understand the contribution of each component. Our proposed StreamDiffusion achieves an average inference time of 10.98/9.42 ms and 26.93/26.30 ms for denoising steps 1 and 4 on image-to-image/text-to-image generation, respectively. When the stream batch processing is removed ('w/o stream batch'), we observe a large time consumption increase, especially at 4 denoising steps. The absence of TensorRT ('w/o TRT') leads to a more increase in time cost. The removal of pre-computation also results in increased time cost but not much. We attribute the reason to the limited number of key-value computations in StableDiffusion. Besides, the exclusion of input-output queue ('w/o IO queue') also demonstrates an impact on average inference time, which mainly aims to optimize the

Table 3. The effect of different modules on average inference time at different denoising steps. The different module ablations are validated on image-to-image generation.

Method	Denoising Step	Latency [ms]
Ours (txt2img)	1	9.42
	4	26.30
Ours (img2img)	1	10.65
	4	26.93
w/o stream batch	1	10.70
	4	36.54
w/o TRT	1	21.34
	4	48.15
w/o Pre-computation	1	13.63
	4	31.16
w/o TinyAutoEncoder	1	49.72
	4	65.48
w/o IO queue	1	15.13
	4	29.72
w/o any optimization	1	76.78
	4	134.37
with SSF	1	10.66
	4	27.02

parallelization issue results from pre- and post-processing. In the AutoPipelineImage2Image’s adding noise function, the precision of tensors is converted from fp32 to fp16 for each request, leading to a decrease in speed. In contrast, the StreamDiffusion pipeline standardizes the precision of variables and computational devices beforehand. It does not perform tensor precision conversion or computation device transfers during inference. Consequently, even without any optimization (‘w/o any optimization’), our pipeline significantly outperforms the AutoPipelineImage2Image in terms of speed. We also evaluate the impact on the inference time of our pipeline with additional modules such as SSF and Self-Negative RCFG. As shown in Table. 2 and Table. 3, these additional modules, which only perform lightweight matrix and vector operations, do not have a noticeable effect on inference time.

4.4. Qualitative Results

The generation results using the StreamDiffusion pipeline for real-time image-to-image transformation are presented in Fig. 1. This pipeline enables image generation with very low throughput from input images received in real time from cameras or screen capture devices. At the same time, it is capable of producing high quality images that effectively align to the specified prompt conditions. These capabilities

demonstrate the applicability of our pipeline in various real time applications, such as real time game graphic rendering, generative camera effect filters, real time face conversion, and AI-assisted drawing.

The alignment of generated images to prompt conditioning using Residual Classifier-Free Guidance (RCFG) is depicted in Fig. 10. The generated images, without using any form of CFG, exhibit weak alignment to the prompt, particularly in aspects like color changes or the addition of non-existent elements, which are not effectively implemented. In contrast, the use of CFG or RCFG enhances the ability to modify original images, such as changing hair color, adding body patterns, and even incorporating objects like glasses. Notably, the use of RCFG results in a stronger influence of the prompt compared to standard CFG. RCFG, although limited to image-to-image applications, can compute the vector for negative conditioning while continuously referencing the latent value of the input image and the initially sampled noise. This approach yields more consistent directions for the negative conditioning vector compared to the standard CFG, which uses UNet at every denoising step to calculate the negative conditioning vector. Consequently, this leads to more pronounced changes from the original image. However, there is a trade-off in terms of the stability of the generated results. While Self-Negative RCFG enhances the prompt’s effectiveness, it also has the drawback of increasing the contrast of the generated images. To address this, adjusting the *delta* in Eq. 7 can modulate the magnitude of the virtual residual noise vector, thereby mitigating the rise in contrast. Additionally, using Onetime-Negative RCFG with appropriately chosen negative prompts can effectively mitigate contrast increases while improving prompt adherence, as observed in Fig. 10. This approach allows the generated images to blend more naturally with the original image.

Finally, the quality of standard text-to-image generation results is demonstrated in Fig. 11. Using the sd-turbo model, high-quality images like those shown in Fig. 11 can be generated in just one step. When images are produced using our proposed StreamDiffusion pipeline and sd-turbo model in an environment with GPU: RTX 4090, CPU: Core i9-13900K, and OS: Ubuntu 22.04.3 LTS, it’s feasible to generate such high-quality images at a rate exceeding 100fps. Furthermore, by increasing the batch size of images generated at once to 12, our pipeline can continuously produce approximately 150 images per second. The images enclosed in red frames shown Fig. 11 are generated in four steps using community models merged with LCM-LoRA. While these LCM models require more than 1 step for high quality image generation, resulting in a reduction of speed to around 40fps, these LCM-LoRA based models offer the flexibility of utilizing any base model, enabling the generation of images with diverse expressions.

5. Conclusion

We propose StreamDiffusion, a pipeline-level solution for interactive diffusion generation. StreamDiffusion consists of several optimization strategies for both throughput and GPU usage, including stream batch, residual classifier-free guidance (RCFG), IO-queue for parallelization, stochastic similarity filter, pre-computation, Tiny AutoEncoder and the use of model acceleration tool. The synergistic combination of these elements results in a marked improvement in efficiency. Specifically, StreamDiffusion achieves up to 91.07 frames per second (fps) on a standard consumer-grade GPU for image generation tasks. This performance level is particularly beneficial for a variety of applications, including but not limited to the Metaverse, online video streaming, and broadcasting sectors. Furthermore, StreamDiffusion demonstrates a significant reduction in GPU power consumption, achieving at least a 1.99x decrease. This notable efficiency gain underscores StreamDiffusion’s potential for commercial application, offering a compelling solution for energy-conscious, high-performance computing environments.

6. Acknowledgments

We sincerely thank Taku Fujimoto and Huggingface team for their invaluable feedback, courteous support, and insightful discussions.

References

- [1] Omri Avrahami, Dani Lischinski, and Ohad Fried. Blended diffusion for text-driven editing of natural images. In *Proceedings of the IEEE/CVF Conference on Computer Vision and Pattern Recognition (CVPR)*, pages 18208–18218, 2022. 3
- [2] Omri Avrahami, Ohad Fried, and Dani Lischinski. Blended latent diffusion. *ACM Trans. Graph.*, 42(4), 2023. 3
- [3] James Betker, Gabriel Goh, Li Jing, TimBrooks, Jianfeng Wang, Linjie Li, LongOuyang, JuntangZhuang, JoyceLee, YufeiGuo, WesamManassra, PrafullaDhariwal, CaseyChu, YunxinJiao, and Aditya Ramesh. Improving image generation with better captions. 2
- [4] Andreas Blattmann, Tim Dockhorn, Sumith Kulal, Daniel Mendelevitch, Maciej Kilian, Dominik Lorenz, Yam Levi, Zion English, Vikram Voleti, Adam Letts, et al. Stable video diffusion: Scaling latent video diffusion models to large datasets. *arXiv preprint arXiv:2311.15127*, 2023. 3
- [5] Andreas Blattmann, Robin Rombach, Huan Ling, Tim Dockhorn, Seung Wook Kim, Sanja Fidler, and Karsten Kreis. Align your latents: High-resolution video synthesis with latent diffusion models. In *Proceedings of the IEEE/CVF Conference on Computer Vision and Pattern Recognition*, pages 22563–22575, 2023. 3
- [6] Yilun Du, Shuang Li, and Igor Mordatch. Compositional visual generation with energy based models. In *Advances in Neural Information Processing Systems*, pages 6637–6647. Curran Associates, Inc., 2020. 4
- [7] Jonathan Ho and Tim Salimans. Classifier-free diffusion guidance. *arXiv preprint arXiv:2207.12598*, 2022. 4
- [8] Jonathan Ho, Ajay Jain, and Pieter Abbeel. Denoising diffusion probabilistic models. *Advances in neural information processing systems*, 33:6840–6851, 2020. 2
- [9] Yushi Huang, Ruihao Gong, Jing Liu, Tianlong Chen, and Xianglong Liu. Tfmcq-dm: Temporal feature maintenance quantization for diffusion models. *arXiv preprint arXiv:2311.16503*, 2023. 2
- [10] Alexia Jolicoeur-Martineau, Ke Li, Rémi Piché-Taillefer, Tal Kachman, and Ioannis Mitliagkas. Gotta go fast when generating data with score-based models. *arXiv preprint arXiv:2105.14080*, 2021. 3
- [11] Diederik P Kingma and Max Welling. Auto-encoding variational bayes, 2022. 7
- [12] Xiuyu Li, Yijiang Liu, Long Lian, Huanrui Yang, Zhen Dong, Daniel Kang, Shanghang Zhang, and Kurt Keutzer. Q-diffusion: Quantizing diffusion models. In *Proceedings of the IEEE/CVF International Conference on Computer Vision (ICCV)*, pages 17535–17545, 2023. 2
- [13] Xingchao Liu, Xiwen Zhang, Jianzhu Ma, Jian Peng, and Qiang Liu. Instaflow: One step is enough for high-quality diffusion-based text-to-image generation. *arXiv preprint arXiv:2309.06380*, 2023. 2
- [14] Cheng Lu, Yuhao Zhou, Fan Bao, Jianfei Chen, Chongxuan Li, and Jun Zhu. Dpm-solver: A fast ode solver for diffusion probabilistic model sampling in around 10 steps. *Advances in Neural Information Processing Systems*, 35:5775–5787, 2022. 2, 3
- [15] Cheng Lu, Yuhao Zhou, Fan Bao, Jianfei Chen, Chongxuan Li, and Jun Zhu. Dpm-solver++: Fast solver for guided sampling of diffusion probabilistic models. *arXiv preprint arXiv:2211.01095*, 2022. 3
- [16] Simian Luo, Yiqin Tan, Longbo Huang, Jian Li, and Hang Zhao. Latent consistency models: Synthesizing high-resolution images with few-step inference, 2023. 2
- [17] Simian Luo, Yiqin Tan, Suraj Patil, Daniel Gu, Patrick von Platen, Apolinário Passos, Longbo Huang, Jian Li, and Hang Zhao. Lcm-lora: A universal stable-diffusion acceleration module. *arXiv preprint arXiv:2311.05556*, 2023. 2, 3, 7
- [18] Simian Luo, Yiqin Tan, Suraj Patil, Daniel Gu, Patrick von Platen, Apolinário Passos, Longbo Huang, Jian Li, and Hang Zhao. Lcm-lora: A universal stable-diffusion acceleration module, 2023. 7
- [19] Aditya Ramesh, Prafulla Dhariwal, Alex Nichol, Casey Chu, and Mark Chen. Hierarchical text-conditional image generation with clip latents. *arXiv preprint arXiv:2204.06125*, 1(2):3, 2022. 3
- [20] Robin Rombach, Andreas Blattmann, Dominik Lorenz, Patrick Esser, and Björn Ommer. High-resolution image synthesis with latent diffusion models, 2021. 3, 7
- [21] Robin Rombach, Andreas Blattmann, Dominik Lorenz, Patrick Esser, and Björn Ommer. High-resolution image synthesis with latent diffusion models. In *Proceedings of the IEEE/CVF conference on computer vision and pattern recognition*, pages 10684–10695, 2022. 2, 7

- [22] Nataniel Ruiz, Yuanzhen Li, Varun Jampani, Yael Pritch, Michael Rubinstein, and Kfir Aberman. Dreambooth: Fine tuning text-to-image diffusion models for subject-driven generation. 2022. [3](#)
- [23] Chitwan Saharia, William Chan, Saurabh Saxena, Lala Li, Jay Whang, Emily Denton, Seyed Kamyar Seyed Ghasemipour, Burcu Karagol Ayan, S. Sara Mahdavi, Rapha Gontijo Lopes, Tim Salimans, Jonathan Ho[†], David Fleet, and Mohammad Norouzi. Imagen: unprecedented photorealism × deep level of language understanding. 2022. [2](#)
- [24] Tim Salimans and Jonathan Ho. Progressive distillation for fast sampling of diffusion models. *arXiv preprint arXiv:2202.00512*, 2022. [3](#)
- [25] Yang Song, Jascha Sohl-Dickstein, Diederik P Kingma, Abhishek Kumar, Stefano Ermon, and Ben Poole. Score-based generative modeling through stochastic differential equations. *arXiv preprint arXiv:2011.13456*, 2020. [2, 3](#)
- [26] Yang Song, Prafulla Dhariwal, Mark Chen, and Ilya Sutskever. Consistency models. *arXiv preprint arXiv:2303.01469*, 2023. [2, 3, 4](#)
- [27] Daniel Watson, Jonathan Ho, Mohammad Norouzi, and William Chan. Learning to efficiently sample from diffusion probabilistic models. *arXiv preprint arXiv:2106.03802*, 2021. [3](#)
- [28] Tianwei Yin, Michaël Gharbi, Richard Zhang, Eli Shechtman, Frédo Durand, William T. Freeman, and Taesung Park. One-step diffusion with distribution matching distillation. *arXiv*, 2023. [2](#)
- [29] Hongkai Zheng, Weili Nie, Arash Vahdat, Kamyar Azizzadenesheli, and Anima Anandkumar. Fast sampling of diffusion models via operator learning. In *International Conference on Machine Learning*, pages 42390–42402. PMLR, 2023. [3](#)